Experimental Thermal and Fluid Science 33 (2009) 1055–1064

Contents lists available at ScienceDirect

Experimental Thermal and Fluid Science

journal homepage: www.elsevier.com/locate/etfs

# Free-surface fluctuations in hydraulic jumps: Experimental observations

Frédéric Murzyn [a], Hubert Chanson [b,*]

[a] ESTACA Campus Ouest, Parc Universitaire de Laval Changé, BP 53061, Laval Cedex 9, France
[b] School of Civil Engineering, The University of Queensland, St. Lucia, Brisbane QLD 4072, Australia

ARTICLE INFO

*Article history:*
Received 16 March 2009
Received in revised form 10 June 2009
Accepted 11 June 2009

*Keywords:*
Hydraulic jumps
Free-surface fluctuations
Frequency
Turbulent shear flow
Air bubble entrainment
Roller length
Experimental techniques

ABSTRACT

A hydraulic jump is the rapid and sudden transition from a high-velocity supercritical open channel flow to a subcritical flow. It is characterised by the dynamic interactions of the large-scale eddies with the free-surface. New series of experimental measurements were conducted in hydraulic jumps with Froude numbers between 3.1 and 8.5 to investigate these interactions. The dynamic free surface measurements were performed with a non-intrusive technique while the two-phase flow properties were recorded with a phase-detection probe. The shape of the mean free surface profile was well defined and the turbulent fluctuation profiles highlighted a distinct peak of turbulent intensity in the first part of the jump roller, with free-surface fluctuation levels increasing with increasing Froude number. The dominant free-surface fluctuation frequencies were typically between 1 and 4 Hz. A comparison between the acoustic sensor signals and conductivity probe data suggested that the air–water "free-surface" detected by the acoustic sensor corresponded to about the boundary between the turbulent shear layer and the upper free-surface layer. Simultaneous measurements of free surface and bubbly flow fluctuations for $Fr = 5.1$ indicated that the frequency ranges of both sensors were similar ($F < 5$ Hz) whatever the position downstream of the toe. The present results highlighted that the dynamic free-surface measurements can be conducted successfully using acoustic displacement meters, and the time-averaged depth measurements was a physical measure of the free-surface location in hydraulic jumps.



## 1. Introduction

Turbulent free-surface flows including hydraulic jumps are characterised by some interfacial aeration (Fig. 1). In the highly aerated flow where the void fraction $C$ ranges from 0.3 to 0.7, the microscopic two-phase flow structure is complex, and it consists of a wide range of entities including air–water projections, foam, and complicated air–water imbrications [23,2]. In high-velocity open channel flows, Killen [10] suggested the possibility of surface waves riding over a bubbly flow region, while Toombes and Chanson [28] studied the influence of surface waves and fluctuations of the flow depth on the two-phase air–water flow properties. Mouaze et al. [18] investigated specifically the free-surface fluctuations in a hydraulic jump roller. Fig. 2 documents some air–water flow structures above a hydraulic jump roller.

A hydraulic jump is the rapid and sudden transition from a high-velocity supercritical open channel flow to a subcritical flow (Fig. 1). Hydraulic jumps are commonly experienced in rivers and canals, in industrial applications and in manufacturing processes. The application of the momentum principle to the hydraulic jump gives a relationship between the flow properties upstream and downstream of a hydraulic jump. In a horizontal rectangular prismatic channel, it yields:

$$\frac{d_2}{d_1} = \frac{1}{2} \times \left( \sqrt{1 + 8 \times Fr^2} - 1 \right) \quad (1)$$

where $d$ and $V$ are the flow depth and velocity respectively, the subscripts 1 and 2 refer to the upstream and downstream flow conditions respectively, $Fr$ is the inflow Froude number: $Fr = V_1/\sqrt{g \times d_1}$, and $g$ is the gravity acceleration. Turbulence measurements in hydraulic jumps were conducted by several researchers, including Rouse et al. [26], Resch and Leutheusser [24], Resch and Leutheusser [25], Chanson and Brattberg [6], Liu et al. [14], Lennon and Hill [12], Chanson [3] and Kucukali and Chanson [11]. These studies focused either on the turbulent water flow properties with relatively low Froude number conditions or on the air–water flow properties in the jump roller. Related experiments investigated the fluctuations of hydraulic jump properties including the toe position and water level [13,16] (Table 1).

In a hydraulic jump, the characterisation of free-surface fluctuations may be conducted with different techniques: e.g., the wire gage and the acoustic displacement sensor. The first kind is particularly accurate for periodic waves in absence of wave breaking as well as details of the free surface turbulence length and time scales for low Froude numbers [18]. When the flow becomes strongly

* Corresponding author. Tel.: +61 7 33653516; fax: +61 7 33654599.
*E-mail address:* h.chanson@uq.edu.au (H. Chanson).
*URL:* http://www.uq.edu.au/~e2hchans/ (H. Chanson).

0894-1777/$ - see front matter © 2009 Elsevier Inc. All rights reserved.
doi:10.1016/j.expthermflusci.2009.06.003

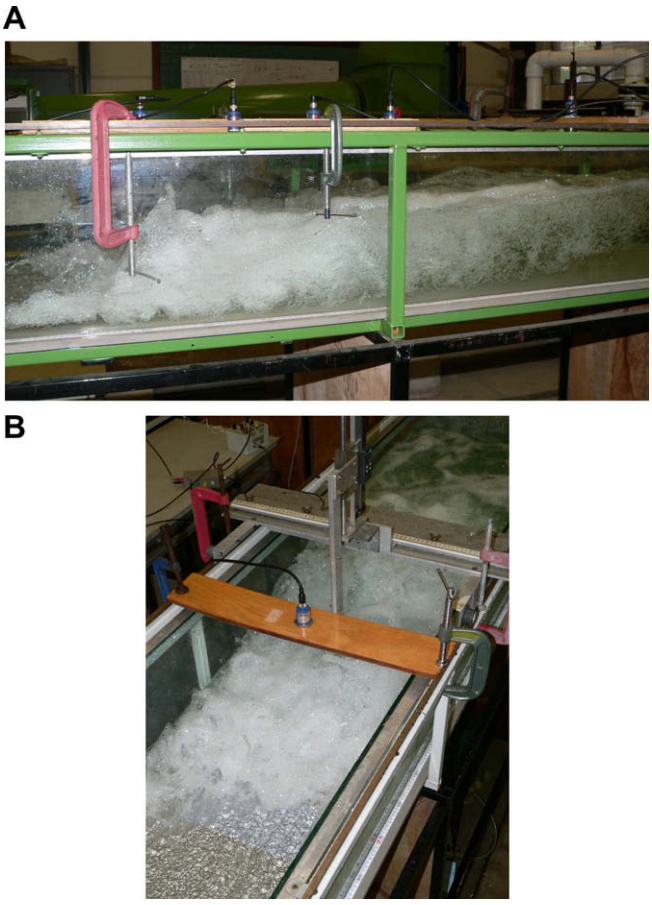


**Fig. 1.** Photographs of a hydraulic jump in the experimental channel. (A) General view: $Fr = 7.9$, $d_1 = 0.018$ m, flow from left to right (shutter: 1/80 s). Note the five acoustic displacement sensors mounted above the channel. (B) General view: $Fr = 7$, $d_1 = 0.024$ m, flow from bottom to top (shutter: 1/80 s). Note the phase detection probe with its sensor located at $x - x_1 = 0.2$ m and the acoustic displacement sensor mounted above.

turbulent with large variations of the air–water interface associated with bubbles, splashes and droplets, the output signal must be considered with some caution because the sensitive part of the probe is not continuously immersed. Further most sensors have a dynamic response that is generally lower than 12 Hz [22]. The second technique (acoustic displacement sensor) is non intrusive (Fig. 1B) and more accurate in terms of the dynamic response. Herein, the sensor manufacturer specified with a response time less than 50 ms. While the acoustic displacement sensor seems a well-defined measurement technique, two key questions remain: what do these sensors exactly measure? What is the accuracy?

In the present study, the free-surface fluctuations and air–water flow properties in hydraulic jumps were investigated. Both acoustic displacement sensors and phase-detection probes were used. It is the aim of this work to assess the suitability of the acoustic displacement sensor, and to examine the free surface motion as well as the air–water flow properties in hydraulic jumps for a relatively broad range of Froude numbers ($3.1 < Fr < 8.5$).

## 2. Experimental set-up and instrumentation

New experiments were performed in a 3.2 m long 0.5 m wide horizontal rectangular flume (Fig. 1, Table 1). The glass sidewalls were 0.45 m high and the channel bed was PVC. The water discharge was measured with a Venturi meter located in the supply line which was calibrated on-site with a large V-notch weir. The clear-water flow depths were measured using rail mounted point gages. The inflow conditions were controlled by a vertical gate with a semi-circular rounded shape ($\varnothing = 0.3$ m). The upstream gate aperture was fixed during all experiments ($d_1 = 0.018$ m).

The unsteady free surface measurements were conducted using six ultrasonic displacement meters Microsonic™ Mic + 25/IU/TC. The acoustic displacement sensors were mounted above the flow at fixed locations for all series of experiments (Fig. 1). Each probe signal output was scanned at 50 Hz per sensor for 10 min (unless stated).

The air–water flow properties were measured with a phase-detection conductivity probe ($\varnothing = 0.25$ mm). The phase-detection intrusive probe was excited by an electronic system (model Ref. UQ82.518) designed with a response time of less than 10 μs. During the experiments, the probe sensor was sampled at 20 kHz for 45 s per sampling point, and each vertical profile contained at least 30 points. The displacement and the position of the probe in the vertical direction were controlled by a fine adjustment system connected to a Mitutoyo™ digimatic scale unit with a vertical accuracy $\Delta y$ of less than 0.1 mm.

Further details on the experimental facility and data sets were reported in Murzyn and Chanson [19].

### 2.1. Signal outputs and processing

The principle of the acoustic displacement meters is based upon an acoustic beam emitted in air by the sensor. Once the beam hits the air–water interface, it is reflected back to the sensor. A simple measure of the travel time provides the distance between the sensor and the free surface. Although the measurement principle is basic, the present experience highlighted a number of situations when the outputs were meaningless. For example, when the free surface was not horizontal, the acoustic beam did not reflect back to the receiver; when the free surface was a bubbly foam, the sensor response might correspond to an unknown location in the intermediate flow region (discussion below); when measurements were made above the roller with a large Froude number, data errors were caused by bubbles, water splashes and droplets coming into contact with the emitter. Herein, the acoustic displacement sensor signal was filtered to remove and replace erroneous points. In most cases, less than 7% of the data samples were also removed. For two data sets, up to 20% were removed due to the large number of droplets impacting the ultrasonic displacement meter sensor.

The analysis of the phase-detection probe output was based upon a single threshold technique, with a threshold set between 45% and 55% of the air–water voltage range [27,7]. A number of air–water flow properties were derived from the signal analysis, including the instantaneous void fraction and the time-averaged void fraction $C$ defined as the volume of air per unit volume of air and water. The sampling rate (20 kHz) and duration (45 s) of the conductivity probe was selected based upon the detailed sensitivity analysis [4]). When the conductivity probe was sampled simultaneously with the displacement sensor, the sampling rate was reduced because the dynamic response of the acoustic displacement meters was much lower, while the sampling duration was not a relevant parameter since the focus of that study was the instantaneous free-surface and void fraction data.

### 2.2. Measurement accuracy and error

The water discharge was measured with an accuracy of about 2%. The clear-water flow depths were measured using a point gage with a 0.2 mm accuracy. The ultrasonic displacement meters had a 0.18 mm accuracy and 50 ms response time. The translation of the conductivity probes in the direction normal to the channel invert was controlled with an error of less than 0.1 mm. The accuracy

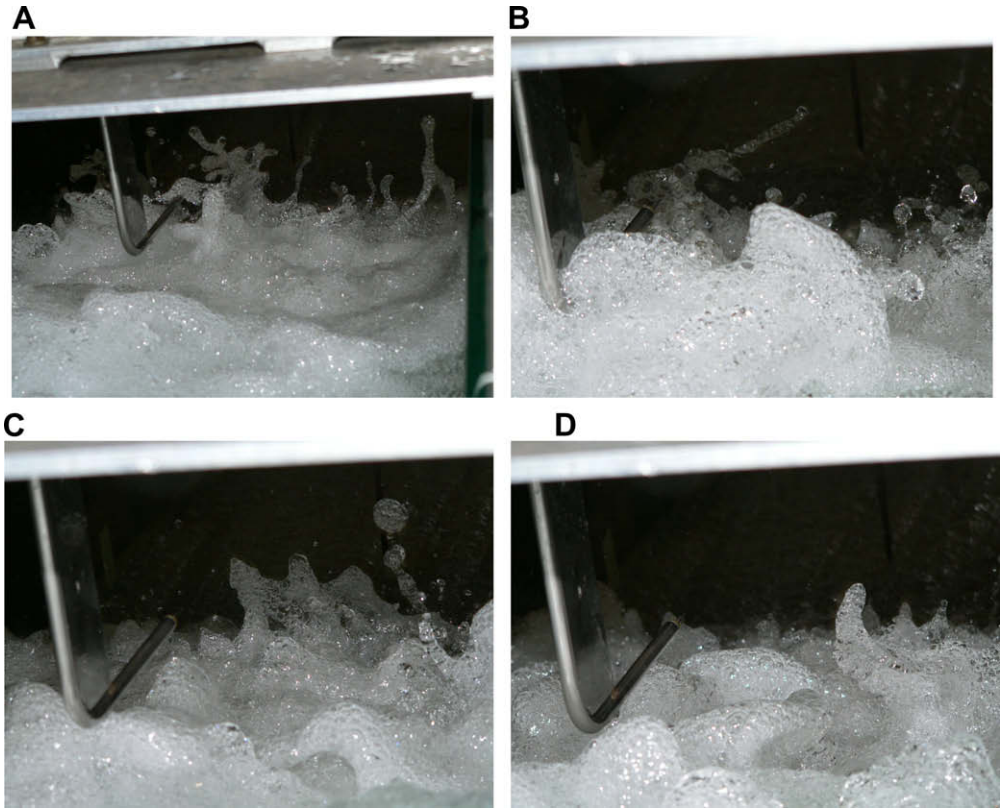


**Fig. 2.** High-speed photographs of the free-surface deformation and water ejections above the hydraulic jump roller, looking upstream towards the toe: $Fr = 8.45$, $d_1 = 0.018$ m, flow from background to foreground (shutter: 1/150 s). Note the phase-detection probe on the left with its tip located at $x - x_1 = 0.225$ m. Each photograph was taken a few second apart.

on the longitudinal probe position was estimated as $\Delta x < \pm 0.5$ cm. The error on the transverse position of the probe was less than 1 mm. With the double-tip conductivity probe, the error on the void fraction measurements was estimated as: $\Delta C/C = 4\%$ for $0.05 < C < 0.95$, $\Delta C \approx 0.002/(1 - C)$ for $C > 0.95$, and $\Delta C/C \approx 0.005/C$ for $C < 0.05$. The minimum detectable bubble chord length was about 50 μm in a 1 m/s flow based upon a data acquisition frequency of 20 kHz per channel.

### 2.3. Experimental flow conditions

The experimental measurements were performed with inflow Froude numbers ranging 3.1–8.5 (Table 1). The corresponding Reynolds numbers ranged from 24 to $64 \times 10^5$, and were large enough to minimise scale effects [8,20].

The jump toe was located at $x_1 = 0.75$ m downstream of the rounded gate, and clear-water velocity measurements showed that the inflow conditions were partially-developed. The downstream flow properties were controlled by an overshoot gate located 2.45 m downstream of the jump toe.

## 3. Experimental results: free-surface fluctuations

Two basic characteristic of the hydraulic jump are its mean longitudinal free surface profile and its free-surface fluctuations. Although the free-surface was well-defined upstream of the toe (nearly flat), it became strongly turbulent downstream of the impingement point with large vertical fluctuations and a bubbly/foamy structure (Figs. 1 and 2). In the roller, high amplitude motions and strong fluctuations in time and space occurred with increasing amplitude with increasing Froude number. Herein the mean and turbulent profiles, as well as the free-surface fluctuation frequencies, are presented first. The measurements were performed using the acoustic displacement meters and were compared with some pertinent studies (Table 1).

Visual observations showed that the air–water interface exhibited some small amplitude motions for the lowest Froude number, whereas it became strongly turbulent for the larger Froude numbers with large air packets and splashes projected above the air–water interface (Fig. 2). Fig. 3 presents some results obtained in terms of the mean free surface profile for six experiments with Froude numbers ranging from 3.1 to 8.5 (Table 1). In Fig. 3, the position of the jump toe corresponds to $(x - x_1)/d_1 = 0$, where $x$ is the longitudinal distance from the upstream gate, and $x_1$ is the toe position, and $\eta$ is the flow depth. Upstream of the jump toe ($x < x_1$), the free surface profile was flat with small fluctuations. The upstream flow depths were between 0.017 m and 0.020 m which were close to the upstream gate aperture ($d_1 = 0.018$ m). The difference of about 10% was satisfactory considering the uncertainties of the sensors and the expected contraction coefficient of unity for the upstream rounded gate. Downstream of the jump toe ($x > x_1$), a monotonic increase of the mean water level was noted. This pattern was in accordance with visual observations during the experiments and photographic evidences (Fig. 1A). For inflow Froude numbers less than 6.5, the jump roller surface was followed by a flat region where the flow was less turbulent: i.e., with large-scale motion and low fluctuation frequencies (Fig. 3). For these jumps ($Fr \leqslant 6.4$), the roller length ($L_r$) was estimated where $L_r$ was defined as the distance over which the mean free surface level increased monotonically. The results are presented in Fig. 4 in terms of the dimensionless roller length ($L_r/d_1$). The present roller length data were in agreement with the experiments of Murzyn et al. [22] ($1.9 < Fr < 4.8$) and the correlation of Hager et al. [9] developed for $2.5 < Fr < 8$ in horizontal rectangular channels.

**Table 1**
Experiment measurements of hydraulic jump fluctuations.

| Reference | $x_1$ (m) | $d_1$ (m) | $Fr$ | $Re$ | $W$ (m) | Instrumentation |
|---|---|---|---|---|---|---|
| Madsen [15] | 0.1 | 0.024 | 2 | 23,000 | 0.15 | Resistance gage |
| Long et al. [13] | 0.042 | 0.025 | 4.0 | 49,200 | 0.47 | High-speed video |
| | 0.082 | | 6.0 | 73,700 | | |
| | 0.081 | | 8.0 | 98,300 | | |
| | 0.077 | | 9.0 | 110,600 | | |
| Mossa and Tolve [17] | 0.9 | 0.020 | 6.4 | 57,000 | 0.45 | PIV and photography |
| Mossa [16] | – | 0.009 to 0.0165 | 1.3 to 8.9 | 17,000 to 54,800 | 0.3 | Electrical probe and video |
| | – | 0.011 to 0.0385 | 3.0 to 9.9 | 30,600 to 122,500 | 0.4 | |
| Liu et al. [14] | – | 0.071 | 2.0 | 118,600 | 0.46 | High-speed video |
| | – | 0.071 | 2.5 | 147,700 | | |
| | – | 0.041 | 3.32 | 86,100 | | |
| Mouaze et al. [18] | 0.35 | 0.059 | 1.98 | 88,230 | 0.30 | Wire gages |
| | | 0.032 | 3.65 | 64,965 | | |
| Murzyn et al. [22] | 0.43 | 0.059 | 2.0 | 87,901 | 0.30 | Wire gage |
| | 0.44 | 0.046 | 2.4 | 74,930 | | |
| | 0.34 | 0.032 | 3.7 | 65,156 | | |
| | 0.36 | 0.021 | 4.8 | 45,679 | | |
| | 0.18 | 0.029 | 2.1 | 32,836 | | |
| | 0.29 | 0.045 | 1.9 | 56,316 | | |
| | 0.43 | 0.059 | 2.0 | 87,901 | | |
| Chanson and Gualtieri [8] | 0.5 | 0.013 | 8.5 | 38,000 | 0.25 | Visual observations and conductivity probes |
| | 1.0 | 0.028 | 4.6 | 69,000 | | |
| | | 0.029 | 5.0 | 77,000 | | |
| | | 0.029 | 6.7 | 100,000 | | |
| | | 0.025 | 7.5 | 94,000 | | |
| | 1.0 | 0.027 | 5.1 | 68,000 | 0.50 | |
| | | 0.028 | 6.9 | 100,000 | | |
| | | 0.027 | 7.3 | 98,000 | | |
| | | 0.024 | 8.6 | 98,000 | | |
| Kucukali and Chanson [11] | 1.0 | 0.024 | 4.7 | 54,335 | 0.50 | Acoustic displacement meters and conductivity probes |
| | | | 5.0 | 57,800 | | |
| | | | 5.8 | 67,050 | | |
| | | | 6.9 | 79,770 | | |
| | | | 8.5 | 98,265 | | |
| Present study | 0.75 | 0.018 | 3.1 | 23,750 | 0.50 | Acoustic displacement meters and conductivity probes |
| | | | 4.2 | 31,850 | | |
| | | | 5.3 | 39,800 | | |
| | | | 6.4 | 48,600 | | |
| | | | 7.6 | 57,050 | | |
| | | | 8.5 | 64,100 | | |

*Notes*: Hydraulic jumps with partially-developed inflow conditions; $d_1$: inflow depth; $Fr$: inflow Froude number; $Re$: Reynolds number defined as $Re = \rho \times V_1 \times d_1/\mu$; $W$: channel width; $x_1$: distance between sluice gate and jump toe; (–): information not available.

### 3.1. Free-surface turbulent fluctuations

The free surface fluctuations were investigated and the results are given in Fig. 5. Fig. 5 presents the dimensionless standard deviation of the water depth $\eta'/d_1$ as a function of the dimensionless distance from the jump toe $(x - x_1)/d_1$. Upstream of the toe, the turbulent fluctuations $\eta'$ were small. Immediately downstream of the jump toe (i.e. $(x - x_1)/d_1 > 0$), a marked increase in free-surface fluctuation was recorded for all Froude numbers, reaching a maximum value $\eta'_{max}$ which increased with increasing Froude number (Fig. 5). Further downstream, the free-surface fluctuations decayed with increasing distance from the jump foot. Far downstream, the turbulence levels were small, with magnitudes comparable to those observed upstream of the impingement point. This pattern was consistent with the earlier studies of Mouaze et al. [18] and Kucukali and Chanson [11], while the downstream decay in free-surface fluctuations would correspond to a dissipative region.

The peak of turbulent fluctuations was observed in the first half of the roller (Fig. 5). This was in agreement with the findings of Mouaze et al. [18] who observed an intense turbulent area with a length of about 30% of the roller length. In the roller region, the flow was characterized by strong turbulence production, large recirculation vortices and coherent structures reaching the free surface. For $Fr = 8.5$, the maximum fluctuation was close to $\eta'_{max}/d_1 = 1.5$ whereas it was only about 0.3 for $Fr = 3.1$ (Fig. 6). The finding highlighted that the free surface motion became more turbulent with increasing inflow Froude number. Since the instantaneous variation in water depth is equal to the vertical velocity component at the free-surface:

$$\frac{\partial \eta}{\partial t} = V_y(y = \eta) \text{ at the free-surface} \quad (2)$$

some algebraical considerations show that the fluctuations of the water depth $\eta$ are linked to the turbulent kinetic energy per unit volume $\varepsilon$: $\eta'^2 \propto v'^2_y \propto \varepsilon$. In a rectangular, horizontal, prismatic channel, the dimensionless rate of energy dissipation equals:

$$\frac{\Delta H}{d_1} = \frac{\left(\frac{d_2}{d_1} - 1\right)^3}{4 \times \frac{d_2}{d_1}} = \frac{\left(\sqrt{1 + 8 \times Fr^2} - 3\right)^3}{16 \times \left(\sqrt{1 + 8 \times Fr^2} - 1\right)} \quad (3)$$

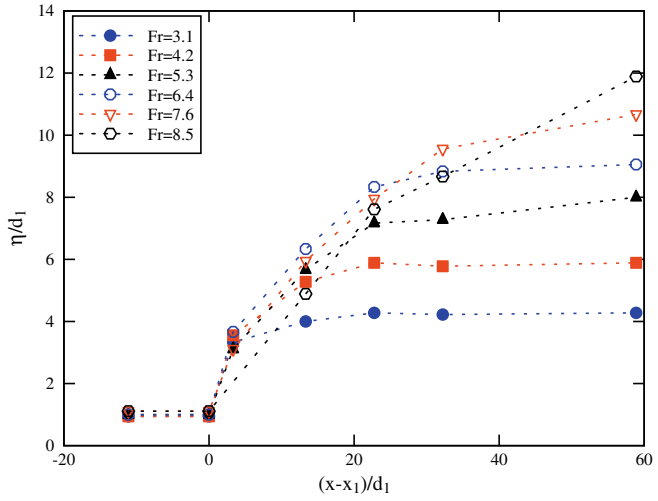


**Fig. 3.** Dimensionless mean free surface profile ($\eta/d_1$) measurements in hydraulic jumps ($Fr$ = 3.1–8.5).

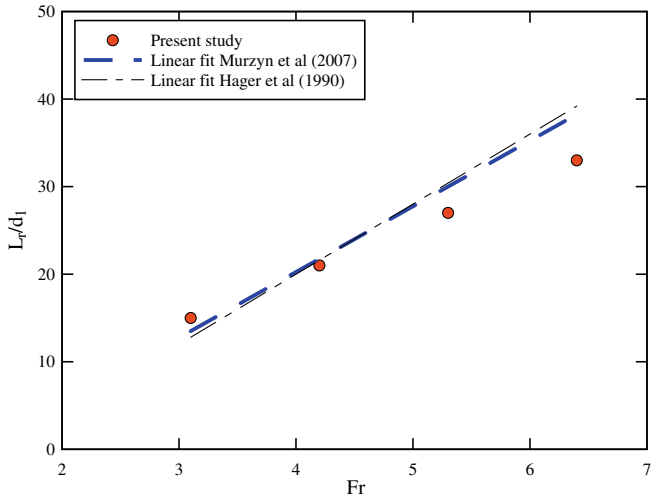


**Fig. 4.** Measurements of dimensionless hydraulic jump roller length $L_r/d_1$ for $Fr$ < 6.5. Comparison with the correlations of Hager et al. [9] and Murzyn et al. [22].

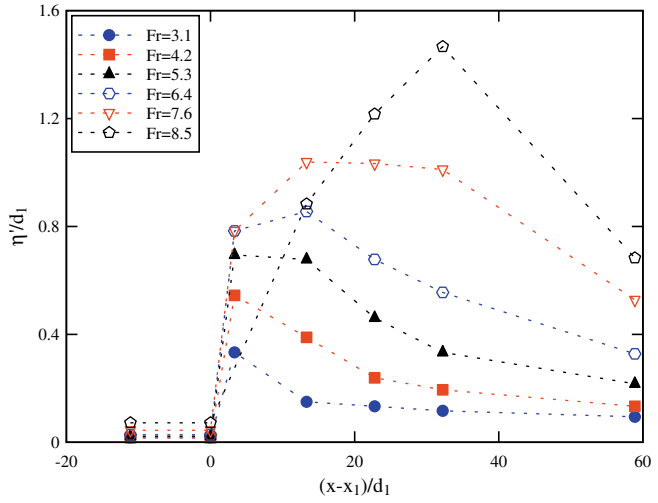


**Fig. 5.** Longitudinal distributions of dimensionless free surface fluctuations $\eta'/d_1$ in hydraulic jumps for several experimental conditions ($Fr$ = 3.1–8.5).

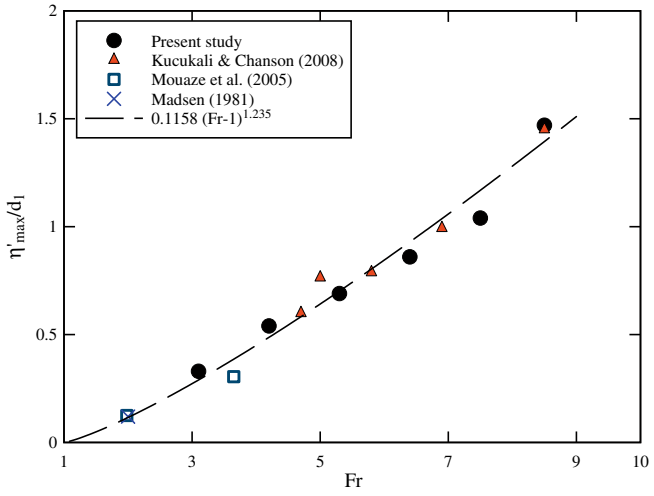


**Fig. 6.** Maximum of turbulent fluctuations $\eta'_{max}/d_1$ in hydraulic jumps as a function of Froude number $Fr$. Comparison with the data of Madsen [15], Mouaze et al. [18] and Kucukali and Chanson [11], and Eq. (4).

For large Froude numbers, it gives: $\Delta H \propto Fr^2$. Combining the continuity equation at the free-surface (Eq. (2)) with the integral form of the energy equation (Eq. (3)), this simple reasoning suggests that, assuming $\Delta H \propto \varepsilon$, the fluctuation of the water level is proportional to the inflow Froude number: $\eta' \propto Fr$. In Fig. 6, the present results are compared with the data of Madsen [15], Mouaze et al. [18] and Kucukali and Chanson [11] (Table 1). The experimental data show that $\eta'_{max} \propto (Fr - 1)$ for $Fr > 5$ and the data trend is identical to the theoretical development.

Overall all the experimental data collapsed into a monotonic curve best fitted by:

$$\frac{\eta'_{max}}{d_1} = 0.116 \times (Fr - 1)^{1.235} \quad (4)$$

with a normalised correlation coefficient of 0.985. Eq. (4) is compared with the experimental data in Fig. 6.

### 3.2. Frequency range(s) in hydraulic jumps

Some spectral analyses of the free-surface fluctuations were performed. The data provided new information on the time scales of the flow next to the free-surface. A typical Fast Fourier Transform (FFT) of a sensor output signal is presented in Fig. 7, where

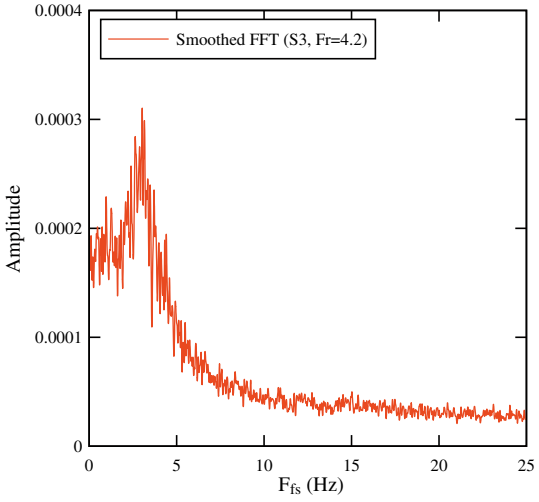


**Fig. 7.** Spectral analysis of the free-surface fluctuations: $Fr$ = 4.2, $d_1$ = 0.018 m, $x_1$ = 0.75 m, $x - x_1$ = 0.24 m.

the smoothed FFT data were obtained using a smoothing window of 20 points. The data highlighted some dominant frequency at the given position downstream of the impingement point. For example, in Fig. 7, a peak is clearly marked at $F_{fs}$ = 3 Hz depicting the main frequency of the free surface fluctuations at $(x - x_1)/d_1$ = 13.3 for $Fr$ = 4.2. This approach was applied to all flow conditions and the results yielded the dominant frequencies of the free-surface fluctuations in the hydraulic jumps. The results are summarised in Table 2 and Fig. 8, where the main frequency data are plotted as a function of the dimensionless distance from the jump toe $(x - x_1)/L_r$ where $L_r$ is the roller length. The graph includes the experimental results obtained in the roller ($(x - x_1)/L_r < 1$) and downstream of the roller ($(x - x_1)/L_r > 1$). Note that the data for $Fr > 6.8$ are not shown because the acoustic displacement meter response was adversely affected by the spray and splashing on the emitter. Fig. 8 indicates that the dominant frequency range was between 1 and 4 Hz. Additional experiments showed little influence of the sampling rate: i.e., 50 Hz during 1200 s, or 5000 Hz for 12 s. For a given inflow Froude number, the free-surface fluctuation frequency appeared to be constant in the hydraulic jump roller $(x - x_1)/L_r < 1$ while $F_{fs}$ decreased downstream for $(x - x_1)/L_r > 1$. Downstream of the jump, the results (Fig. 8) were in good agreement with visual observations.

The horizontal oscillations of the jump toe were also recorded and the data are reported in Table 2. The dimensionless results are plotted in Fig. 9 in terms of the Strouhal number defined as

$$St_{toe} = \frac{F_{toe} \times d_1}{V_1} \quad (5)$$

where $F_{toe}$ is the toe oscillation frequency. The Strouhal number is a dimensionless term characterising the oscillations of a physical system. The results in terms of jump toe oscillation frequencies were compared with the dimensionless free-surface fluctuation frequencies $St_{fs}$ in the jump roller and with two earlier studies of jump toe oscillations (Table 2, Fig. 9). The present data were close to the findings of Mossa and Tolve [17] and Chanson and Gualtieri [8] with steady jumps. It is noteworthy that the range of fluctuation frequency was similar to the free-surface fluctuation frequency observation of Mossa [16] in an oscillating hydraulic jump and turbulent velocity fluctuations of Liu et al. [14] in weak jumps.

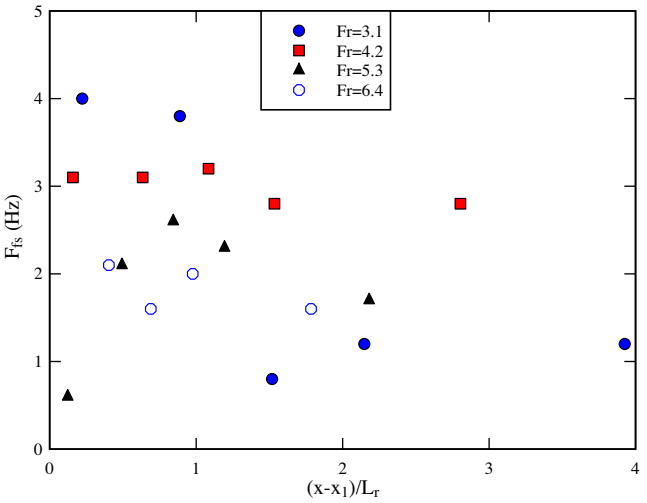


**Fig. 8.** Dominant free surface frequencies $F_{fs}$ of the free-surface fluctuations in hydraulic jumps.

The jump toe oscillation frequencies were consistently smaller than the free-surface fluctuation frequencies for a given Froude number (Fig. 9). The results indicated that the Strouhal number $F_{toe} \times d_1/V_1$ of the toe oscillations was nearly constant independently of the Reynolds number $\rho \times V_1 \times d_1/\mu$, whereas the Strouhal number $F_{fs} \times d_1/V_1$ of the roller surface fluctuations decreased with increasing Reynolds number. These results were in agreement with the earlier observations of Mossa and Tolve [17].

## 4. Discussion: definition of the free-surface

What did the acoustic displacement meter detect? The hydraulic jump roller was highly aerated. Fig. 10A presents typical vertical distributions of void fraction along the roller for a given Froude number. The air bubble entrainment occurred at the impingement of the supercritical flow into the roller. Bubbles and air packets were entrained at the flow singularity and were advected down-

**Table 2**
Experimental observations of jump toe longitudinal oscillations and free-surface oscillations.

| Reference | $x_1$ (m) | $d_1$ (m) | $Fr$ | $F_{toe}$ (Hz) | $St_{toe}$ | $F_{fs}$ (Hz) | $St_{fs}$ |
|---|---|---|---|---|---|---|---|
| Long et al. [13] | 0.082 | 0.025 | 6 | – | 0.062 (∗) | | |
| | 0.081 | 0.025 | 8 | – | 0.023 (∗) | | |
| | 0.077 | 0.025 | 9 | – | 0.033 (∗) | | |
| Mossa and Tolve [17] | 0.90 | 0.020 | 6.4 | 0.67 | 0.0047 | – | – |
| Mossa [16] | – | 0.0287 | 4.52 | – | – | 1–3 | 0.015–0.045 |
| Chanson and Gualtieri [8] | 0.5 | 0.013 | 8.5 | 1.27 | 0.0055 | – | – |
| | 1.0 | 0.028 | 4.6 | 0.59 | 0.0069 | – | – |
| | | 0.029 | 5.0 | 0.75 | 0.0081 | – | – |
| | | 0.029 | 6.7 | 1.18 | 0.0096 | – | – |
| | | 0.025 | 7.5 | 1.27 | 0.0086 | – | – |
| | 1.0 | 0.027 | 5.1 | 1.25 | 0.013 | – | – |
| | | 0.028 | 6.9 | 1.47 | 0.011 | – | – |
| | | 0.027 | 7.3 | 1.59 | 0.011 | – | – |
| | | 0.024 | 8.6 | 2.0 | 0.011 | – | – |
| Present study | 0.75 | 0.018 | 3.1 | – | – | 3.83 | 0.053 |
| | | | 4.2 | – | – | 3.14 | 0.032 |
| | | | 5.1 | 0.47 | 0.0040 | – | – |
| | | | 5.3 | – | – | 2.35 | 0.019 |
| | | | 6.4 | – | – | 1.13 | 0.0076 |
| | | | 7.6 | 0.68 | 0.0038 | – | – |
| | | | 8.3 | 0.77 | 0.0039 | – | – |

*Notes*: Hydraulic jumps with partially-developed inflow conditions; $F_{fs}$: free-surface fluctuation dominant frequency; $F_{toe}$: jump toe oscillation frequency; $St$: Strouhal number defined as $St = F \times d_1/V_1$; (∗): large vortical structure angular frequency; (–): data not available.

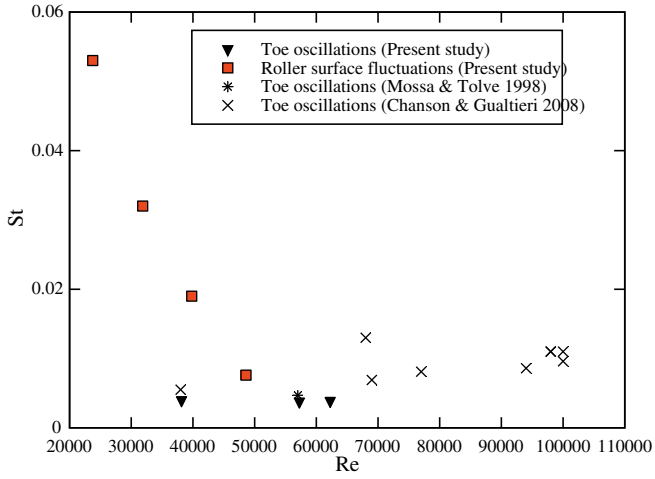


**Fig. 9.** Dimensionless hydraulic jump toe oscillation frequency $F_{toe} \times d_1/V_1$ and dimensionless free-surface fluctuation frequency $F_{fs} \times d_1/V_1$ in hydraulic jumps. Comparison with the jump toe oscillation data of Mossa and Tolve [17] and Chanson and Gualtieri [8].

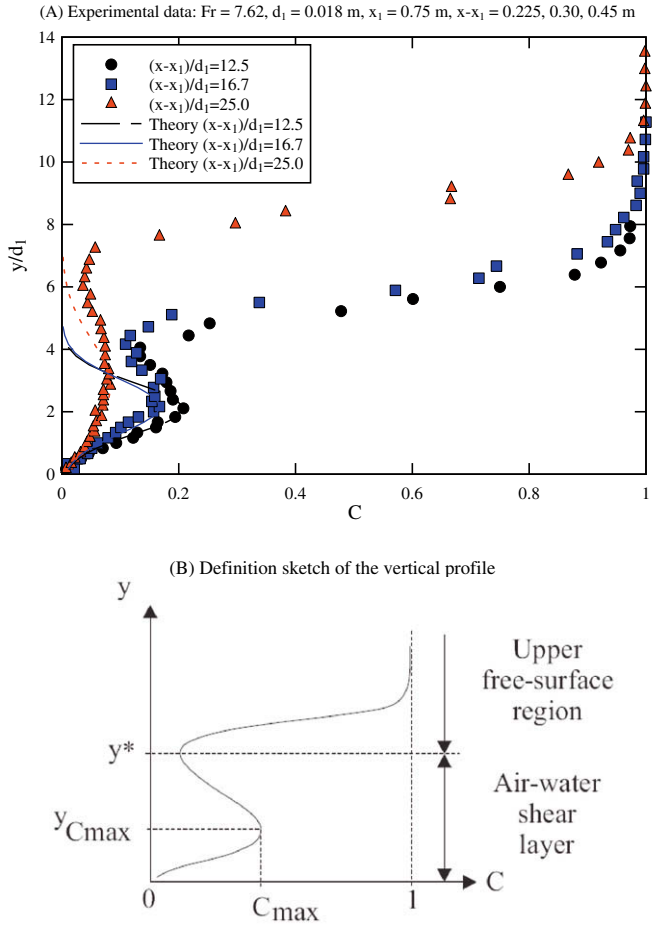


**Fig. 10.** Vertical distributions of void fraction in a hydraulic jump with partially-developed inflow. (A) Experimental data: $Fr = 7.62$, $d_1 = 0.018$ m, $x_1 = 0.75$ m, $x - x_1 = 0.225$, 0.30, 0.45 m. (B) Definition sketch of the vertical profile.

stream in the turbulent shear flow. In the developing shear layer, the data compared favourably with an analytical solution of the advective diffusion equation for air bubbles [1,2] :

$$C = C_{max} \times \exp\left(-\frac{\left(\frac{y-y_{C_{max}}}{d_1}\right)^2}{4 \times D^* \times \left(\frac{x-x_1}{d_1}\right)}\right) \quad (6)$$

where $C_{max}$ is the maximum void fraction in the shear layer, $y_{C_{max}}$ is the vertical elevation of the maximum void fraction $C_{max}$, $D^*$ is a dimensionless turbulent diffusivity. Eq. (6) is compared with some data in Fig. 10. Such a close agreement was previously observed in hydraulic jumps with partially-developed inflow conditions, including a re-analysis of the data of Resch and Leutheusser [25], Chanson and Brattberg [6], Murzyn et al. [21] and Chanson [3].

Above the turbulent shear layer, the upper free-surface region was characterized by large air contents, splashes and recirculation areas, with large eddies, a wavy free surface pattern and air–water projections (Fig. 2). The void fraction profiles illustrated the two distinct regions (Fig. 10B), and $y^*$ is defined herein as the transition between the upper flow region and the air–water shear flow.

### 4.1. Detection of the air–water interface

The present data were analysed to bring new information on the free surface fluctuation characteristics in hydraulic jumps. The relationship between turbulent fluctuation $\eta'_{max}/d_1$ and the maximum amplitude of the free surface $\Delta\eta/d_1$ was tested, where $\Delta\eta$ was the free-surface fluctuation range recorded during the sampling duration ($\Delta\eta = \eta_{max} - \eta_{min}$). The results indicated that the largest turbulent fluctuations were closely linked to the most important free surface amplitudes according to a well-defined linear trend, and this trend was consistent with visual observations.

Two earlier studies tested acoustic displacement sensors above bubbly flows. In a bubbly column with up to 10% void fraction, Chanson et al. [5] observed that the ultrasonic probe readings corresponded to about $y_{50}$–$y_{60}$ where $y_{xx}$ is the elevation where the void fraction is $xx$%. Kucukali and Chanson [11] reported that the response of acoustics displacement meters corresponded to the range $y_{60}$–$y_{80}$ in hydraulic jumps. Herein a comparative analysis was conducted systematically between the acoustic displacement meter and void fraction data. The time-averaged depth recorded with the acoustic displacement meter was compared with the void fraction profile measured with the leading tip of the dual-tip conductivity probe. Some results are presented in Fig. 11. Fig. 11 shows that the time-averaged "free-surface" elevation $\eta$ measured by the acoustic displacement sensor was slightly above the characteristic location $y^*$ for all investigated Froude numbers. The finding

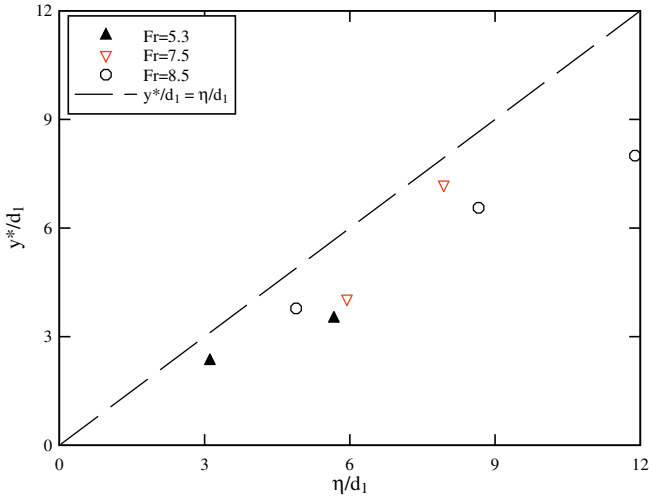


**Fig. 11.** Comparison of free surface and void fraction measurements using acoustic displacement sensor and phase detection probe. Experimental results.

suggested that the interface measurement by the acoustic sensor was within the upper flow region ($\eta > y^*$, Fig. 10B). This region was typically a thin layer where the void fraction was basically larger than 20%, rapidly reaching 90% and more (Fig. 10). The present description is thought to be a more physical measure of the free-surface location in hydraulic jumps because it refers to a specific region of the flow. Altogether, the present findings were in agreement with the experimental data of Kucukali and Chanson [11].

### 4.2. Simultaneous measurements of free-surface and bubbly flow properties

For one Froude number ($Fr = 5.1$), simultaneous measurements of free surface fluctuations and air–water flow properties were conducted using an acoustic displacement meter mounted directly above the phase-detection probe control leading tip as shown in Fig. 1B. The sampling rate was 5000 Hz, the acquisition duration was 12 s for both sensors and the experimental flow conditions are summarised in Table 3. Although the measurements were performed at several different vertical elevations, the comparative results are focused herein on the air–water flow properties at $y = y_{30}$ (i.e. $C = 0.3$).

**Table 3**
Experimental conditions for simultaneous measurements of free surface fluctuations and bubbly flow properties.

| $Fr$ | $d_1$ (m) | $x_1$ (m) | $x - x_1$ (m) | $(x - x_1)/d_1$ | Nb points | $y_{30}/d_1$ |
|---|---|---|---|---|---|---|
| 5.1 | 0.018 | 0.75 | 0.090 | 5.0 | 10 | 3.50 |
| | | | 0.165 | 9.17 | 9 | 4.83 |
| | | | 0.240 | 13.33 | 9 | 5.67 |

*Note*: Nb points = number of experiments with phase-detection probe at different vertical elevations.

The spectral analyses were performed on the processed signals of both sensors. The original output signal was filtered using a band pass (0–25 Hz) and the low-pass filtered signal was averaged over 100 points. Fig. 12 presents a comparison between the raw probe signal (phase-detection probe only) and the processed signals. Fig. 12B illustrates the time-series of simultaneous processed signals. Typical results of spectral analyses are presented in Fig. 13. In Fig. 13, the FFT analysis of the phase detection probe signal is on the left and that of the free-surface signal on the right. The results showed that the dominant frequencies were less than 5 Hz for both conductivity probe and acoustic displacement sensors (Fig. 13), implying that the bubble generation and free surface vertical motion might be dependant processes.

A cross-correlation analysis was performed on the processed signals of both phase detection probe and acoustic sensor. Typical cross correlation functions, for the two conditions shown in Fig. 13,

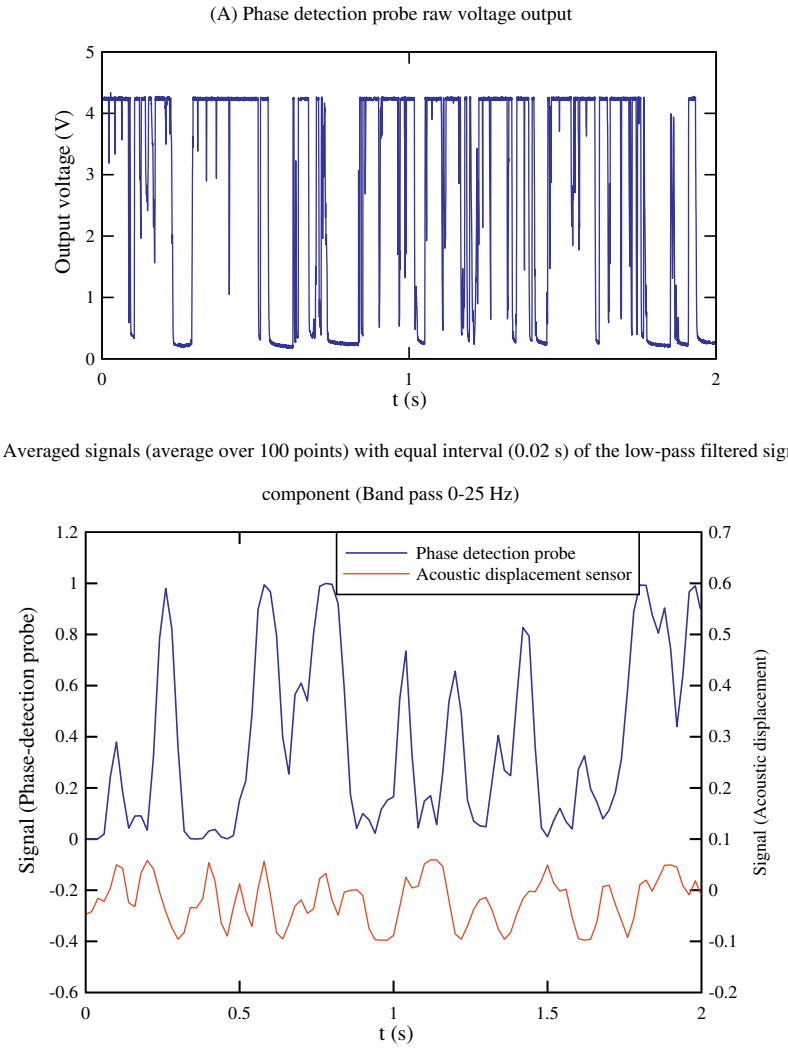


**Fig. 12.** Simultaneous measurements of free-surface and bubbly flow properties. Flow conditions: $Fr = 5.1$, $(x - x_1)/d_1 = 5.0$, $y/d_1 = 3.5$. (A) Phase detection probe raw voltage output. (B) Averaged signals (average over 100 points) with equal interval (0.02 s) of the low-pass filtered signal component (band pass 0–25 Hz).

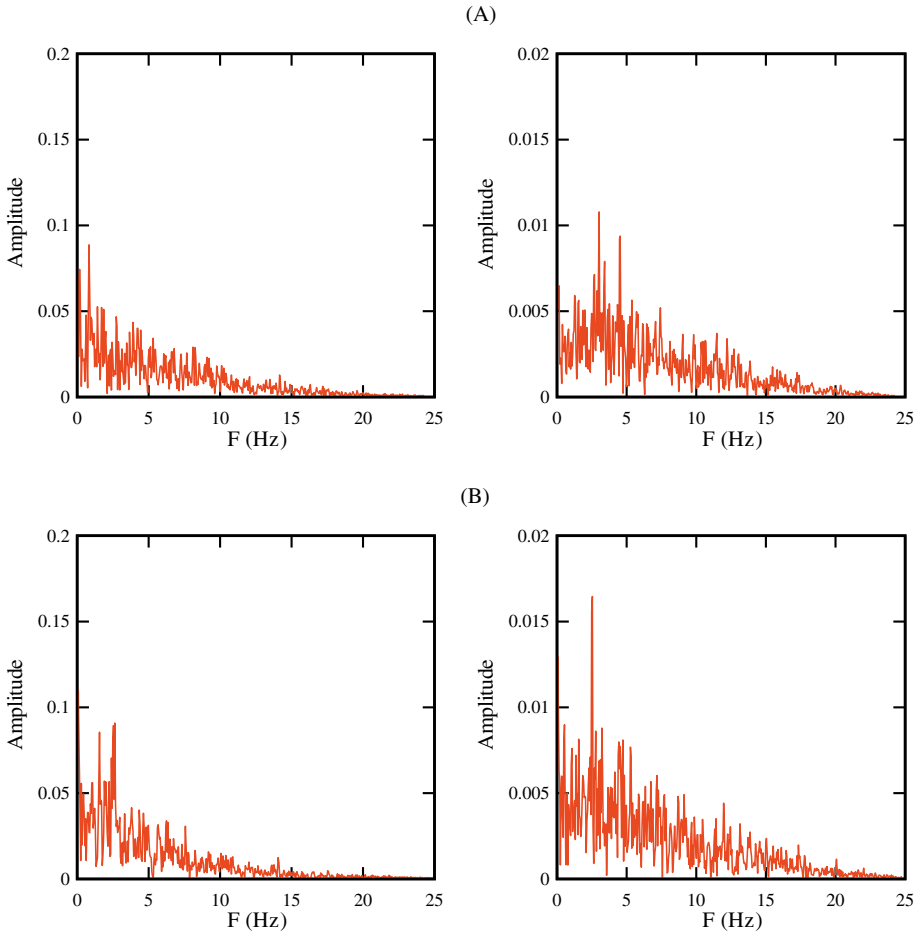


**Fig. 13.** Spectral analyses (FFT) of both phase-detection probe and acoustic displacement sensor signals – flow conditions: $Fr = 5.1$ – (left) conductivity probe signal; (right) acoustic displacement sensor signal. (A) $(x - x_1)/d_1 = 5.0$, $y/d_1 = 3.5$. (B) $(x - x_1)/d_1 = 13.33$, $y/d_1 = 5.67$.

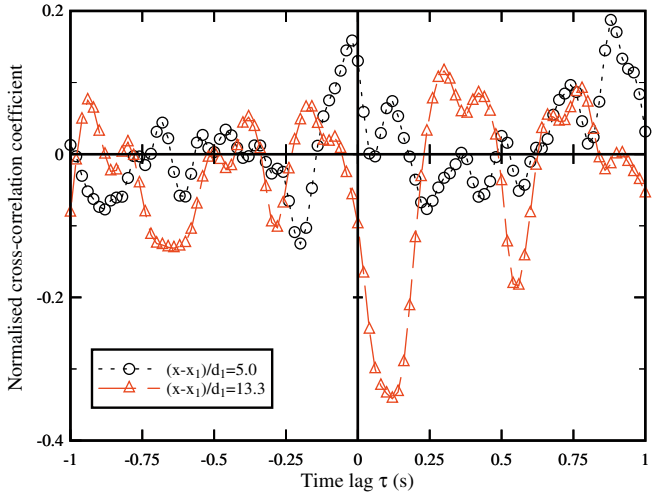


**Fig. 14.** Normalised cross-correlation functions between the conductivity probe signal and acoustic displacement meter sensor. Flow conditions: $Fr = 5.1$.

are presented in Fig. 14. In Fig. 14, the vertical axis is the normalised coefficient of correlation $R_{xz}$ where $x$ is the phase-detection probe signal and $z$ is the free-surface fluctuation signal, and the horizontal axis is the time lag. Altogether the results exhibited some large negative and positive values with some periodic shape (Fig. 14). A spectral analysis of these cross-correlation functions revealed that the dominant frequencies were 1.12 Hz, 1.56 Hz and 2.34 Hz for $(x - x_1)/d_1 = 5.0$, 9.2 and 13.3 respectively. These values were consistent with results presented earlier herein.

## 5. Conclusion

In a hydraulic jump, the large vortices develop beneath the free-surface and are advected in the developing shear layer. The interactions of the large-scale eddies with the free-surface yield a complex two-phase flow structure, consisting of a wide range of entities including air–water projections, foam, and complicated air–water imbrications. Some new series of experimental measurements were conducted in hydraulic jumps with Froude numbers between 3.1 and 8.5 to characterise the turbulent free-surface fluctuations. Dynamic free surface measurements were performed with non-intrusive acoustic displacement meters while the two-phase flow properties were recorded with a phase-detection probe. For one Froude number, instantaneous free surface and void fraction data were simultaneously recorded to study some correlation between their respective frequency ranges.

For Froude numbers between 3.1 and 8.5, the shape of the mean free surface profile was well defined and the results were in agreement with visual observations and earlier studies. The turbulent fluctuation profiles highlighted a distinct peak of turbulent intensity in the first part of the jump roller, and the peak of free-surface fluctuation levels increased with increasing Froude number. The free-surface fluctuation frequencies were typically between 1 and 4 Hz. The dominant frequency was typically higher in the roller

than in the downstream flow. It was consistently larger than the jump toe oscillation frequency for $Fr < 5.3$, but tended to comparable values for larger Froude numbers ($Fr > 5.3$) (Fig. 9). A comparison between the acoustic sensor and phase-detection probe signals suggested that the air–water "free-surface" detected by the acoustic sensor corresponded to about the boundary between the turbulent shear layer and the upper free-surface layer ($\eta \sim y^*$).

Simultaneous measurements of free surface and bubbly flow fluctuations for $Fr = 5.1$ were performed. The spectral analyses indicated that the frequency ranges of both sensors were similar ($F < 5$ Hz) whatever the position downstream of the toe. The signal cross correlations showed some large positive and negative values implying with some periodic shapes. The findings suggested the air bubble entrainment and free surface vertical motion might be dependant processes.

Ultimately, the present results highlighted that the dynamic free-surface measurements can be conducted successfully using acoustic displacement meters, and the time-averaged depth measurements was a physical measure of the free-surface location in hydraulic jumps. The data hinted furthermore some interactions between the free-surface fluctuations and the two-phase flow properties of the developing shear flow, although further investigations are needed.

## Acknowledgments

The writers thank Mr Graham ILLIDGE for his technical assistance, Professor Michele Mossa for his advice and comments, and Mr François Stéphan for his support. They acknowledge the financial assistance of the ESTACA and Australian Research Council.

## References

[1] H. Chanson, Air entrainment in two-dimensional turbulent shear flows with partially developed inflow conditions, International Journal of Multiphase Flow 21 (6) (1995) 1107–1121.
[2] H. Chanson, Air bubble entrainment in free-surface turbulent shear flows, Academic Press, London, UK, 1997. 401p..
[3] H. Chanson, Bubbly flow structure in hydraulic jump, European Journal of Mechanics B/Fluids 26(3) (2007) 367–384, doi: 10.1016/j.euromechflu.2006.08.001.
[4] H. Chanson, Dynamic similarity and scale effects affecting air bubble entrainment in hydraulic jumps, in: M. Sommerfield (Ed.), Proceedings of the 6th International Conference on Multiphase Flow ICMF 2007, Leipzig, Germany, July 9–13, Session 7, Paper S7_Mon_B_S7_Mon_B_3, 11 pages (CD-ROM), 2007.
[5] H. Chanson, S. Aoki, M. Maruyama, Unsteady air bubble entrainment and detrainment at a plunging breaker: dominant time scales and similarity of water level variations, Coastal Engineering 46 (2) (2002) 139–157.
[6] H. Chanson, T. Brattberg, Experimental study of the air–water shear flow in a hydraulic jump, International Journal of Multiphase Flow 26 (4) (2000) 583–607.
[7] H. Chanson, G. Carosi, Advanced post-processing and correlation analyses in high-velocity air–water flows, Environmental Fluid Mechanics 7(6) (2007) 495–508, doi: 10.1007/s10652-007-9038-3.
[8] H. Chanson, C. Gualtieri, Similitude and scale effects of air entrainment in hydraulic jumps, Journal of Hydraulic Research, IAHR 46 (1) (2008) 35–44.
[9] W.H. Hager, R. Bremen, N. Kawagoshi, Classical hydraulic jump: length of roller, Journal of Hydraulic Research, IAHR 28 (5) (1990) 591–608.
[10] J.M. Killen, The Surface Characteristics of Self-aerated Flow in Steep Channels, Ph.D. Thesis, University of Minnesota, Minneapolis, USA, 1968.
[11] S. Kucukali, H. Chanson, Turbulence measurements in hydraulic jumps with partially-developed inflow conditions, Experimental Thermal and Fluid Science 33(1) (2008) 41–53, doi: 10.1016/j.expthermflusci.2008.06.012.
[12] J.M. Lennon, D.F. Hill, Particle image velocimetry measurements of undular and hydraulic jumps, Journal of Hydraulic Engineering, ASCE 132 (12) (2006) 1283–1294.
[13] D. Long, N. Rajaratnam, P.M. Steffler, P.R. Smy, Structure of flow in hydraulic jumps, Journal of Hydraulic Research, IAHR 29 (2) (1991) 207–218.
[14] M. Liu, N. Rajaratnam, D.Z. Zhu, Turbulent structure of hydraulic jumps of low Froude numbers, Journal of Hydraulic Engineering, ASCE 130 (6) (2004) 511–520.
[15] P.A. Madsen, A Model for a Turbulent Bore, Ph.D. Thesis, Technical University of Denmark, Institute of Hydrodynamics and Hydraulic Engineering, Copenhagen, Denmark, 1981, 149p. (also Series Paper No. 28, Technical University of Denmark, Institute of Hydrodynamics and and Hydraulic Engineering, Copenhagen, Denmark, 149p.)
[16] M. Mossa, On the oscillating characteristics of hydraulic jumps, Journal of Hydraulic Research, IAHR 37 (4) (1999) 541–558.
[17] M. Mossa, U. Tolve, Flow visualization in bubbly two phase hydraulic jumps, Journal of Fluids Engineering, Transactions of the ASME 120 (1998) 160–165.
[18] D. Mouaze, F. Murzyn, J.R. Chaplin, Free surface length scale estimation in hydraulic jumps, Journal of Fluids Engineering, Transactions of the ASME 127 (2005) 1191–1193.
[19] F. Murzyn, H. Chanson, Free surface, bubbly flow and turbulence measurements in hydraulic jumps, Report No. CH63/07, Division of Civil Engineering, The University of Queensland, Brisbane, Australia, July, 2007, 116p.
[20] F. Murzyn, H. Chanson, Experimental assessment of scale effects affecting two-phase flow properties in hydraulic jumps, Experiments in Fluids 45(3) (2008) 513–521, doi: 10.1007/s00348-008-0494-4.
[21] F. Murzyn, D. Mouaze, J.R. Chaplin, Optical fibre probe measurements of bubbly flow in hydraulic jumps, International Journal of Multiphase Flow 31 (1) (2005) 141–154.
[22] F. Murzyn, D. Mouaze, J.R. Chaplin, Air–water interface dynamic and free surface features in hydraulic jumps, Journal of Hydraulic Research, IAHR 45 (5) (2007) 679–685.
[23] N.S.L. Rao, H.E. Kobus, Characteristics of self-aerated free-surface flows. Water and Waste Water/Current Research and Practice, vol. 10, 1971, Eric Schmidt Verlag, Berlin, Germany.
[24] F.J. Resch, H.J. Leutheusser, Le Ressaut Hydraulique: mesure de Turbulence dans la Région Diphasique, ('The Hydraulic Jump: Turbulence Measurements in the Two-Phase Flow Region'), La Houille Blanche, No. 4, 1972, pp. 279–293 (in French)
[25] F.J. Resch, H.J. Leutheusser, Reynolds stress measurements in hydraulic jumps, Journal of Hydraulic Research, IAHR 10 (4) (1972) 409–429.
[26] H. Rouse, T.T. Siao, S. Nagaratnam, Turbulence characteristics of the hydraulic jump, Transactions, ASCE 124 (1959) 926–966.
[27] L. Toombes, Experimental Study of Air–Water Flow Properties on Low-Gradient Stepped Cascades, Ph.D. Thesis, Department of Civil Engineering, The University of Queensland, Brisbane, Australia, 2002
[28] L. Toombes, H. Chanson, Surface waves and roughness in self-aerated supercritical flow, Environmental Fluid Mechanics 5(3) (2007) 259–270, doi: 10.1007/s10652-007-9022-y.